Journal of Geodesy (2020) 94:47
https://doi.org/10.1007/s00190-020-01374-8

ORIGINAL ARTICLE

Fusing adjacent-track InSAR datasets to densify the temporal resolution of time-series 3-D displacement estimation over mining areas with a prior deformation model and a generalized weighting least-squares method

Yuedong Wang[1] · Zefa Yang[1] · Zhiwei Li[1] · Jianjun Zhu[1] · Lixin Wu[1]

Received: 25 August 2019 / Accepted: 11 April 2020 / Published online: 23 April 2020

Abstract
Interferometric synthetic aperture radar (InSAR) technology can be used to observe high spatial resolution one-dimensional (1-D) deformation along the line-of-sight direction from a single-track synthetic aperture radar (SAR) dataset. With the aid of multi-track InSAR data or a prior model, InSAR can be extended to infer 3-D deformation information, but the temporal resolution is generally limited. This paper presents an InSAR-based method to retrieve high spatio-temporal resolution 3-D displacements over mining areas (hereafter referred to as the *MTI-based method*). The core idea of the proposed method is to enhance the temporal resolution of the time-series 3-D displacement estimates by fusing multi-track InSAR observations and a prior model. Firstly, we retrieve high spatial resolution 3-D mining displacements from single-track InSAR 1-D deformation observations, with the assistance of the prior deformation model. By applying this approach to multi-track InSAR data over the same area, we obtain much denser 3-D mining displacement samples in time than those derived from a single-track InSAR dataset. Secondly, we propose a generalized weighted least-squares method to integrate the denser 3-D displacement samples, to solve the high temporal resolution 3-D mining displacements, in which the rank deficiency needs to be tackled. Finally, time-series 3-D mining displacements at the chronological dates of all the available multi-track SAR images are estimated. The Yungang coal mining area of China was selected to test the proposed method using two adjacent-track ALOS PALSAR-1 datasets. Compared with the single-track InSAR-derived results, the proposed method not only significantly improves the temporal resolution of the monitoring results by 42.6%, obtaining more detailed 3-D displacements, but it also provides important data support for understanding and modeling the distinctive kinematics of mining deformation and assessing mining-related geohazards. What is more, the core idea of the proposed method will be beneficial to high spatio-temporal resolution 3-D deformation estimation in other geophysical processes.

Keywords InSAR · 3-D deformation · Mining subsidence · Time series · Prior deformation model

1 Introduction

Ground surface deformation is an important indicator for Earth's geophysical phenomena such as volcanoes, earthquakes, glacier movement, and fault movement. Therefore, ground surface three-dimensional (3-D) displacement observations with high spatial and temporal resolutions are essential for geophysical process studies (e.g., parameterization of deformation systems, forward modeling, and inverse modeling), because the higher the spatial and temporal resolutions of the 3-D displacement observations are, the more the details of the progressive deformation and its patterns in space and time can be revealed. To this end, researchers have focused on improving or even revolutionizing conventional geodetic and/or new remote sensing techniques over recent decades, so that one can observe high spatial and temporal resolution ground surface 3-D time-series (or dynamic) displacements in a wide area at a low cost (e.g., Mohr et al. 1998; Catalao et al. 2011; Hu et al. 2012).

Compared with large-scale geophysical deformation studies, high spatio-temporal resolution 3-D displacement obser-

✉ Zefa Yang
yangzf@csu.edu.cn

[1] School of Geosciences and Info-Physics, Central South University, Changsha 410083, Hunan, China

vations are more important for local mining deformation studies, for the following reasons. Ground surface displacements caused by mining activities (especially coal extraction) are usually characterized by high speed and high nonlinearity in space and time (Peng et al. 1992; Reddish and Whittaker 2012) over a small area (e.g., several square kilometers). As a result, mining-related geohazards (e.g., infrastructure damage and landslides) are progressively formed with highly spatio-temporal nonlinearity (Marschalko et al. 2012; Yang et al. 2018b). To better understand mining deformation kinematics and reliably assess mining-induced geohazards, time-series three-dimensional (3-D) mining displacement observations with both high spatial and temporal resolution measurements are essential. In contrast, if the spatio-temporal resolution of the observations is too coarse, some critical transient deformations (e.g., the maximum horizontal strain and deformation velocity) are likely to be missed. This significantly impedes deformation kinematics modeling and mining-related geohazard assessment and may even cause wrong results. A more detailed discussion of this issue is provided in Sect. 4.1.

The interferometric synthetic aperture radar (InSAR) technique is capable of monitoring surface displacements with a high spatial resolution (e.g., meters or even less) in a wide area at a low cost. As a result, it has been widely used to monitor the surface deformation associated with geophysical deformation events (e.g., earthquakes, volcanic eruptions, permafrost thawing) and anthropogenic activities (e.g., underground fluid and mineral extraction) (Ryder et al. 2007; Neri et al. 2009; Fournier et al. 2010; Lu et al. 2010; Zhao et al. 2016; Liu et al. 2018; Liu and Xu 2019; Chaussard et al. 2014; Yang et al. 2017a). However, due to the side-looking imaging configuration of the current SAR sensors, only time-series one-dimensional (1-D) deformation along the line-of-sight (LOS) direction can be measured by InSAR from a single-track SAR dataset. This significantly impedes InSAR-based deformation kinematics modeling and geohazard assessment, because time-series 1-D LOS displacement observations cannot reveal or can miss the real dynamic patterns of mining-induced surface deformation occurring in 3-D space. This implies that there is a challenging demand to retrieve time-series 3-D mining displacements from InSAR 1-D measurements. Unfortunately, the published research work is still insufficient.

In 2013, Samsonov et al. (2013) reconstructed 2-D mining time-series displacements in the vertical and east directions in the Greater Region of Luxembourg, using a method termed the Multi-dimensional Small-Baseline Subset (MSBAS) technique (Samsonov and d'Oreye 2012) from multi-track InSAR datasets (i.e., ascending and descending Envisat Advanced Synthetic Aperture Radar (ASAR), as well as descending European Remote Sensing (ERS) datasets). Theoretically, the MSBAS method can fully retrieve time-series 3-D displacements from InSAR datasets with at least three independent imaging geometries. However, due to the near-polar orbits of the current SAR satellites, the independent imaging geometries of the current multi-track and/or multi-sensor (called multi-track for simplification) spaceborne InSAR datasets in most areas (except for polar regions of Earth) are ascending and descending. This means that it is currently very difficult to accurately retrieve time-series 3-D mining displacements from multi-track InSAR observations.

To circumvent this, Yang et al. (2018a) proposed a novel method termed single-geometry InSAR (SGI) for fully retrieving time-series 3-D mining displacements by integrating single-track InSAR observations with a mining-related deformation model. The core idea behind the SGI method is to construct two theoretical constraints related to the 3-D mining displacements based on the prior deformation model, to stabilize the ill-posed problem of estimating time-series 3-D mining displacements from InSAR 1-D deformation observations. Given the fact that the single-track InSAR datasets required in the SGI method can be readily obtained in practice, Yang et al. were able to completely retrieve time-series 3-D mining displacements from InSAR observations. However, due to the long repeat cycles of the current SAR satellites (from more than 10 to dozens of days, in general), the temporal sampling density of single-track SAR datasets is generally low, causing a poor temporal resolution for the SGI-derived results, even though single-track SAR images can be regularly collected. Readers can refer Yang et al. 2020 to a review on InSAR-based retrieval of 3-D mining displacements.

Thanks to the increasing number of available SAR satellites, InSAR datasets from multi-track are now available for areas of interest on the Earth's surface. On the one hand, as mentioned previously, the nature of the two independent imaging geometries of multi-track InSAR datasets over most areas impedes the full retrieval of time-series 3-D mining displacements using the MSBAS method. On the other hand, multi-track SAR datasets have a higher temporal sampling density of surface deformation evolution than single-track datasets, offering great potential in dramatically enhancing the temporal resolution of time-series 3-D mining displacements. Unfortunately, to date, studies exploiting this potential have not been conducted.

In this paper, we propose an approach for estimating time-series 3-D mining displacements by fusing multi-track InSAR (MTI) observations, with the assistance of a prior deformation model. Hereafter, for simplification, we refer to this approach as the *MTI-based method*. The main aim of the MTI-based method is to significantly enhance the temporal resolution of time-series 3-D mining displacement estimates by the use of multi-track InSAR observations, rather than single-track ones, as in the previous SGI method. In addition, a mathematically rigorous coherence-based weighting

scheme, rather than the empirical one (i.e., cubic of coherence) used in the SGI method, is developed to improve the accuracy of time-series 3-D mining displacement estimates. Finally, a special case study of the Yungang coal mining area of China is provided in this paper, where time-series 3-D mining displacements with densified temporal resolution were retrieved using the MTI-based method from two spatially adjacent ascending Advanced Land Observing Satellite (ALOS) Phased Array type L-band Synthetic Aperture Radar (PALSAR)-1 datasets.

2 Methodology

The MTI-based method consists of two main steps. Firstly, it forms small-baseline InSAR pairs from each available multi-track SAR image dataset over the mining area of interest and then generates multi-track 3-D deformation observations from each formed InSAR pair by fusing the InSAR observations and the prior deformation model used in the previous SGI method. A specially developed mathematically rigorous coherence-based weighting scheme is then used to mitigate the error propagation of the observations. By integrating this weighting scheme, a generalized weighted least-squares (GWLS) solver is used to tackle the rank-deficient problem of estimating time-series 3-D mining displacements from multi-track 3-D deformation observations.

2.1 Deriving 3-D mining displacement measurements with a prior deformation model

2.1.1 Generating 1-D LOS deformation observations for each track

We let K ($K \geq 1$) be the number of tracks of all the available SAR image datasets over the same region of interest (ROI). Small-baseline InSAR pairs are then formed from the SAR images of each track by setting different thresholds of spatio-temporal baselines. Each of the formed small-baseline InSAR pairs is then processed with the differential InSAR (DInSAR) technique to generate multi-track 1-D LOS deformation observations, namely $\boldsymbol{L} = [\boldsymbol{L}_1, \boldsymbol{L}_2, \ldots, \boldsymbol{L}_K]$, where $\boldsymbol{L}_i$ ($i = 1, 2, \ldots, K$) denotes the observations of the whole differential interferogram generated from the ith track InSAR dataset.

2.1.2 Retrieving 3-D mining displacement measurements with a prior deformation model, track by track

Since reconstructing 3-D mining displacements from InSAR 1-D LOS deformation observations is an ill-posed problem, the prior deformation model of the mining-induced horizontal motions being linearly proportional to the gradients of the vertical subsidence in the corresponding directions is introduced to stabilize this ill-posed problem. We first construct two theoretical constraint equations related to the 3-D mining displacements, based on the prior model, i.e., (Li et al. 2015),

$$\begin{cases} E = B_{\mathrm{E}} \cdot S_{\mathrm{E}} \\ N = B_{\mathrm{N}} \cdot S_{\mathrm{N}} \end{cases} \tag{1}$$

where E and N are the 2-D horizontal motions in the east and north directions, respectively; S_{E} and S_{N} are the gradients of the vertical subsidence in the east and north directions, respectively; and B_{E} and B_{N} denote the linear proportional coefficients in the corresponding directions.

These two constraint equations are then integrated with the InSAR-derived 1-D LOS deformation observations, to resolve the 3-D displacements. More specifically, for a generic jth InSAR pair from the ith track (whose LOS deformation is denoted by $\boldsymbol{L}_i^j$), the 3-D mining displacements during the time period of this InSAR pair (i.e., $\boldsymbol{W}_i^j$, $\boldsymbol{E}_i^j$, and $\boldsymbol{N}_i^j$) can be estimated by:

$$\begin{cases} \boldsymbol{W}_i^j = \boldsymbol{B}_i^j \cdot \boldsymbol{L}_i^j \\ \boldsymbol{E}_i^j = \boldsymbol{C}_{\mathrm{E}i}^j \cdot \hat{\boldsymbol{W}}_i^j \\ \boldsymbol{N}_i^j = \boldsymbol{C}_{\mathrm{N}i}^j \cdot \hat{\boldsymbol{W}}_i^j \end{cases} \tag{2}$$

where $\boldsymbol{B}_i^j$, $\boldsymbol{C}_{\mathrm{E}i}^j$, and $\boldsymbol{C}_{\mathrm{N}i}^j$ are the coefficient matrices of these three equation systems, which depend on the parameters of the SAR sensors, the resolution of the 1-D LOS deformation maps, and the geological conditions for the mining. $\hat{\boldsymbol{W}}_i^j$ denotes the estimates of the vertical subsidence, which can be solved from the first system in Eq. (2). Please refer to Li et al. (2015) and Yang et al. (2018a) for more details about the solving procedure.

Having processed each of the above generated vectors of the multi-track LOS deformation observations with the above method, we obtain the vectors of the multi-track 3-D mining displacements, namely $\boldsymbol{W} = [\boldsymbol{W}_1, \boldsymbol{W}_2, \ldots, \boldsymbol{W}_K]$, $\boldsymbol{E} = [\boldsymbol{E}_1, \boldsymbol{E}_2, \ldots, \boldsymbol{E}_K]$, and $\boldsymbol{N} = [\boldsymbol{N}_1, \boldsymbol{N}_2, \ldots, \boldsymbol{N}_K]$ in the vertical, east, and north directions, respectively. It is noted that the reference dates and time periods of each 3-D displacement observation in the vectors of $\boldsymbol{W}$, $\boldsymbol{E}$, and $\boldsymbol{N}$ are likely to be different, due to the formation of the multi-track small-baseline InSAR pairs. This implies that unification of the reference date of these multi-track 3-D displacement vectors needs to be carried out to retrieve 3-D time-series mining displacements.

2.2 Estimating time-series 3-D displacements with the method of generalized weighted least squares

Prior to estimating the time-series 3-D mining displacements from the multi-track 3-D displacement observations, two factors should be taken into account, i.e., the nature of the high nonlinearity of mining deformation and the aim of enhancing the temporal resolution of time-series 3-D displacements. To this end, the core idea of numerical integration is introduced to achieve the goal of simultaneously considering these two factors. Since the estimation procedures of time-series 3-D displacements are the same in the vertical, east, and north directions in the MTI-based method, we take the time-series subsidence estimation as an example to comprehensively illustrate the solving steps of time-series 3-D mining displacements.

2.2.1 Constructing the observation system for 3-D displacement velocity estimation

We let p be the number of all the multi-track SAR images, $\boldsymbol{t} = \left[t_1, t_2, \ldots, t_p\right]$ is their chronological date vector, and $\boldsymbol{V}_{\mathrm{W}} = \left[V_{\mathrm{W}1}, V_{\mathrm{W}2}, \ldots, V_{\mathrm{W}p-1}\right]^{\mathrm{T}}$ is the subsidence velocity vector between each two time-adjacent SAR images; that is, $V_{\mathrm{W}i} = \left[W(t_{i+1}) - W(t_i)\right] / \left[t_{i+1} - t_i\right]$, where $W(t_{i+1})$ and $W(t_i)$ denote the time-series subsidence at the dates of t_{i+1} and t_i, respectively. For a surface point of the ROI, its observation system involving multi-track subsidence observations $\boldsymbol{W}$ and subsidence rates $\boldsymbol{V}_{\mathrm{W}}$ can be constructed as:

$$\begin{bmatrix} \boldsymbol{A}_1 \\ \boldsymbol{A}_2 \\ \vdots \\ \boldsymbol{A}_K \end{bmatrix} \cdot \boldsymbol{V}_{\mathrm{W}} = \begin{bmatrix} \boldsymbol{W}_1 \\ \boldsymbol{W}_2 \\ \vdots \\ \boldsymbol{W}_K \end{bmatrix} + \boldsymbol{\delta}_{\mathrm{W}} \text{ or } \boldsymbol{A}\boldsymbol{V}_{\mathrm{W}} = \boldsymbol{W} + \boldsymbol{\delta}_{\mathrm{W}} \tag{3}$$

where $\boldsymbol{A}_i$ is the sub-coefficient matrix of $\boldsymbol{A}$, which depends on the formation network of the ith track small-baseline InSAR pair (Berardino et al. 2002); and $\boldsymbol{\delta}$ denotes the error term of the system [Eq. (3)], mainly depending on the model errors and the uncertainties of LOS displacement observations, see Yang et al. (2018a) for more details.

2.2.2 Developing a mathematically rigorous coherence weighting scheme

The observations in the system [Eq. (3)] derive from multi-track InSAR observations. This implies that the accuracy of the multi-track subsidence observations may differ significantly, due to the different noise levels and different imaging geometries of multi-track SAR datasets. Therefore, a suitable weighting scheme is essential for ensuring the reliability of the solutions of the subsidence velocity vector. However, since no redundant observations are used to solve multi-track 3-D displacements [see Eq. (2)], the variances of the 3-D displacement estimates cannot be determined with the classical adjustment methods. Therefore, other strategies for variance estimation need to be developed for weighting the multi-track 3-D displacement measurements with different levels of accuracy.

In this paper, the 3-D mining displacement estimates are solved from InSAR 1-D deformation observations, whose errors, to a large extent, depend on interferometric coherence. This suggests that coherence could be an important indicator for the variance of 3-D mining displacement estimates. Although Yang et al. (2018a) took the cubic of the coherence to weight single-track 3-D mining displacements in the SGI method, such a weighting scheme is too empirical to effectively mitigate error propagation, especially for multi-track 3-D displacements with significant accuracy differences.

To circumvent this, we propose a mathematically rigorous coherence-based weighting scheme. According to Hanssen (2001), the phase variance δ_ϕ^2 of InSAR can be approximately estimated by:

$$\delta_\phi^2 = \int_{-\pi}^{+\pi} [\phi - E(\phi)]^2 \mathrm{pdf}(\phi) \mathrm{d}\phi \tag{4}$$

where ϕ represents the interference phase of $[-\pi, \pi]$; $E(\phi)$ denotes the expected value of ϕ; and $\mathrm{pdf}(\phi)$ is the probability density function of ϕ, which is related to the interferometric coherence, the multi-look number, etc. (Hanssen 2001). Since LOS deformation is estimated by $L = \lambda / 4\pi \cdot \phi$, the variance of the LOS deformation observation can be denoted by $\delta_{\mathrm{L}}^2 = \left(\lambda / 4\pi\right)^2 \cdot \delta_\phi^2$.

If we assume that the variances of the LOS deformation observations derived from the multi-track InSAR pairs are independent, then the variance–covariance matrix of the LOS observation vector derived from a generic small-baseline InSAR pair can be denoted by $\boldsymbol{D}_{\mathrm{L}} = \mathrm{diag}\left[\delta_{\mathrm{L}}^2(1,1), \delta_{\mathrm{L}}^2(1,2), \ldots, \delta_{\mathrm{L}}^2(m,n)\right]$ (where m and n represent the pixels of the ROI). Accordingly, the variance–covariance matrix of the multi-track 3-D displacement estimates derived from a single InSAR pair can be determined based on the law of error propagation and Eq. (2), i.e.,

$$\begin{cases} \boldsymbol{D}_{\mathrm{W}} = \boldsymbol{B} \cdot \boldsymbol{D}_{\mathrm{L}} \cdot (\boldsymbol{B})^{\mathrm{T}} \\ \boldsymbol{D}_{\mathrm{E}} = \boldsymbol{C}_{\mathrm{E}} \cdot \boldsymbol{D}_{\mathrm{W}} \cdot (\boldsymbol{C}_{\mathrm{E}})^{\mathrm{T}} \\ \boldsymbol{D}_{\mathrm{N}} = \boldsymbol{C}_{\mathrm{N}} \cdot \boldsymbol{D}_{\mathrm{W}} \cdot (\boldsymbol{C}_{\mathrm{N}})^{\mathrm{T}} \end{cases} \tag{5}$$

Having obtained the variance–covariance matrices of the multi-track 3-D displacement estimates using Eq. (5), the weighting matrix for Eq. (3) can also be constructed according to classical adjustment theory (i.e., $P_{\mathrm{W}} = 1 / D_{\mathrm{W}}$, $P_{\mathrm{E}} = 1 / D_{\mathrm{E}}$, $P_{\mathrm{N}} = 1 / D_{\mathrm{N}}$). It should be pointed out that

errors of the LOS deformation observations caused by atmospheric delay and orbital uncertainty cannot be considered in this weighting scheme. Therefore, the atmospheric phase components and the orbital errors contained in the interferometry should be mitigated at the earliest stage (e.g., by polynomial fitting), prior to estimating the 3-D displacements from InSAR-derived LOS displacements.

2.2.3 Solving 3-D displacement velocity vectors using the method of generalized weighted least squares

The observations in the equation system [Eq. (3)] are derived from multi-track InSAR datasets, which causes rank deficiency (Hanssen 2001; Berardino et al. 2002). Therefore, a GWLS solver (Campbell and Meyer 1979), rather than the weighted least-squares (WLS) solver used in the previous SGI method, is proposed to solve the subsidence velocity vector $\hat{\boldsymbol{V}}$ from the rank-deficient observation system [Eq. (3)], i.e.,

$$\hat{\boldsymbol{V}} = (\boldsymbol{A}^{\mathrm{T}}\boldsymbol{P}\boldsymbol{A})^{+}\boldsymbol{A}^{\mathrm{T}}\boldsymbol{P}\Delta\boldsymbol{W} \tag{6}$$

where $(\boldsymbol{A}^{\mathrm{T}}\boldsymbol{P}\boldsymbol{A})^{+}$ denotes the Moore–Penrose pseudoinverse of matrix $\boldsymbol{A}^{\mathrm{T}}\boldsymbol{P}\boldsymbol{A}$. $\boldsymbol{P}$ is the weighting matrix determined with the method described in Sect. 2.2.2.

2.2.4 Estimating time-series 3-D displacements

Having obtained the subsidence rate vector $\hat{\boldsymbol{V}}$ between each two time-adjacent multi-track SAR acquisitions, the time-series vertical subsidence at the dates of the multi-track SAR images $\hat{\boldsymbol{W}} = \left[\hat{W}(t_2),\ \hat{W}(t_3),\ \cdots,\ \hat{W}(t_p)\right]$, with reference to the earliest date (i.e., $\hat{W}(t_1) \equiv 0$), can thus be estimated by:

$$\hat{W}(t_i) = \sum_{k=2}^{i}(t_k - t_{k-1}) \cdot \hat{V}_{k-1}, \quad (i = 2, 3, \ldots, p) \tag{7}$$

It should be pointed out that the above-described estimation procedure for time-series vertical subsidence is on a pixel-by-pixel basis. In addition, although only the estimation procedure of the time-series vertical subsidence is demonstrated above, 2-D horizontal motions in the east and north directions can be estimated using the same procedure. The flowchart of the MTI-based method is shown in Fig. 1.

3 Experiments and results

3.1 Study area

The Yungang coal mining area of Datong, Shanxi province, China (see Fig. 2a), was selected to test the proposed MTI-based method. The reasons for selecting this study area are as follows. Firstly, the long-term and large-scale coal extraction has resulted in serious geohazards (i.e., landslides, structural damage, and land subsidence) in this coal mining area (Jia et al. 2010; Zhao et al. 2011). Hence, there is an urgent need to retrieve time-series 3-D displacements with a high spatio-temporal resolution to assess and control the related geohazards in this area. Furthermore, the Yungang coal mining area has a special geological condition, i.e., the coal seams have hard roofs and the coal itself is also hard (Xie and Zhou 2008). The so-called double hard coal seam geological condition gives rise to some distinctive deformation patterns, such as sinkholes, rock bursts, and mining-caused earthquakes (Lu et al. 2013; Dou et al. 2014; Zhao et al. 2012; Zhu 2015). Consequently, it is of great importance to obtain time-series 3-D displacement observations with a high spatio-temporal resolution to understand the distinctive deformation mechanism and provide forward guidance to geohazard control.

In fact, Yang et al. (2018a) retrieved estimates of the time-series 3-D displacements in the Yungang coal mining area between July 1, 2007, and May 18, 2008, using the SGI method with seven single-track ALOS PALSAR-1 images (frame: 790; path: 454). However, limited by the long repeat cycle of the PALSAR-1 satellite, the mean temporal resolution of the derived time-series 3-D mining displacement estimates is about 54 days. The 54-day temporal resolution is too coarse to be applied to understand mining deformation kinematics and to reliably assess mining-related geohazards (especially for sinkholes, rock bursts, and mining-caused earthquakes) in the Yungang mining area. To clearly show the mining activities, we plotted the geolocations of underground working panels (namely WP 1, 2, and 3) in the concerned mining area during June 14, 2007, and May 18, 2008, in Fig. 2b. It can be seen that the mining activity was carried out in WP1 and WP2 (marked by white rectangles), and the areas marked by green dashed lines denote the mined-out (abandoned) areas.

3.2 SAR dataset and data processing

3.2.1 SAR dataset

In addition to the seven ascending PALSAR-1 SAR images (frame: 790; path: 454) used in Yang et al. (2018a), the Yungang coal mining area is also covered by other SAR images from different tracks (e.g., a spatially adjacent track of PALSAR-1) and different sensors (e.g., Envisat ASAR and RADARSAT) during the same period. Unfortunately, due to the fast speed of the surface deformation in this mining area, severe phase decorrelation occurs in the interferograms generated by these C-band ASAR and RADARSAT SAR images. In this case, nearly all the ASAR and RADARSAT InSAR pairs are unsuitable to accurately detect surface defor-

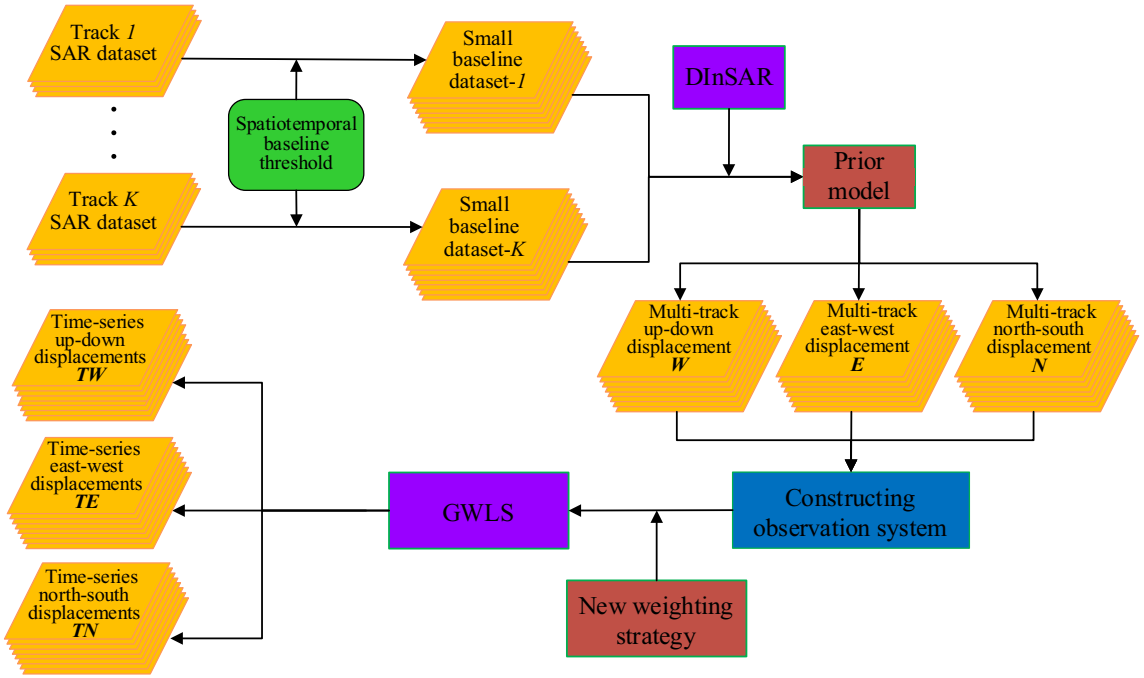

Fig. 1 Flowchart of the MTI-based method

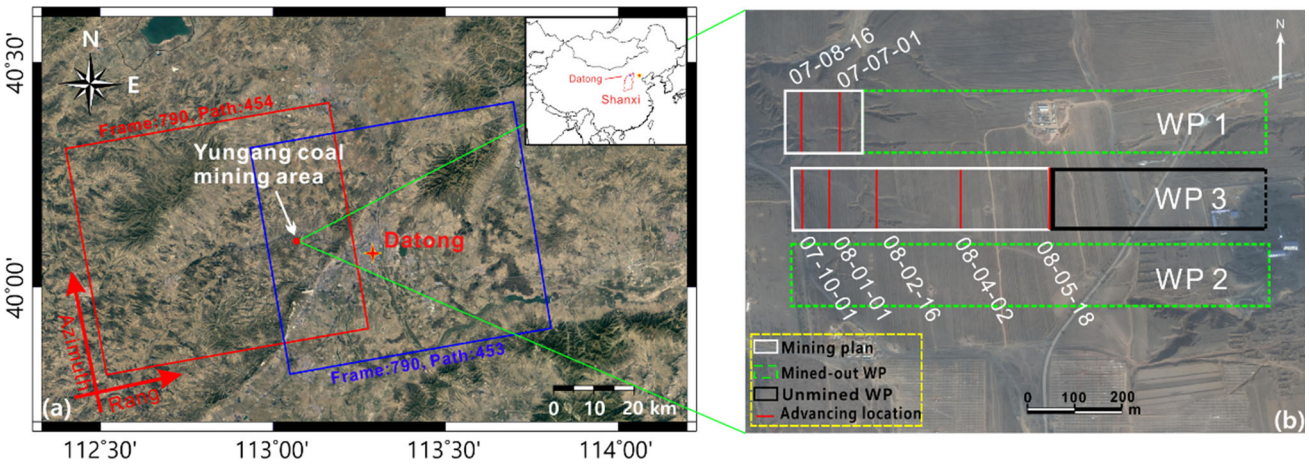

Fig. 2 **a** Geographic location of the Yungang coal mining area (marked by the red point) and the footprints of the left track (frame: 790; path: 454, marked by the red rectangle) and right track (frame: 790; path: 453, marked by the blue rectangle) ALOS PALSAR-1 SAR acquisitions superimposed on the optical image acquired on March 14, 2016. **b** Advancing locations of the working panels overlain on the optical image in the periods of SAR acquisitions. The green dashed, black, and white solid rectangles denote the mined-out, unmined, and planned mining areas of this working face, respectively

mation in the Yungang coal mining area. Fortunately, owing to the longer wavelength of the L-band PALSAR-1 images, the coherence of the small-baseline PALSAR-1 InSAR pairs from the spatially adjacent track (with frame 790 and path 453, see the blue rectangle in Fig. 2a) is acceptable for deformation detection. Therefore, we attempted to enhance the temporal resolution of the time-series 3-D mining displacements in the study area by fusing two spatially adjacent ALOS PALSAR-1 images. For simplification, we refer to the track of frame 790 and path 454 (as used in Yang et al. (2018a)) as the left track (LT), and we refer to the newly fused spatially adjacent track (frame: 790; path: 453) as the right track (RT).

3.2.2 Data processing

Due to the different imaging geometries, we first formed small-baseline InSAR pairs from the LT and RT SAR

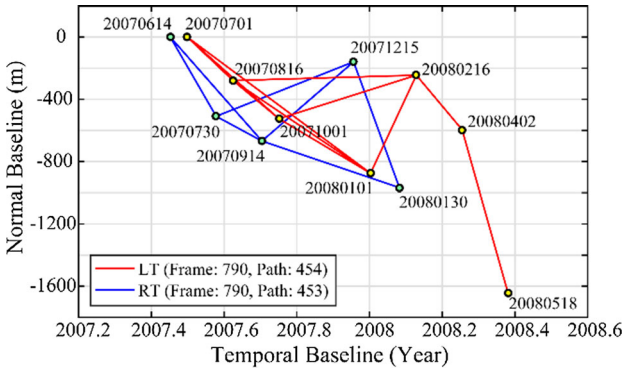

Fig. 3 Temporal and perpendicular baseline network of the available InSAR pairs from the LT (marked by the red lines) and RT (marked by the blue lines) tracks

datasets, respectively, with the same spatio-temporal baseline thresholds of 140 days and 1500 m. After the elimination of those small-baseline InSAR pairs with severe spatio-temporal phase decorrelation (by visual interpretation), we formed 11 and seven InSAR pairs from the LT and RT SAR images, respectively. The perpendicular and temporal baseline network of the available LT and RT InSAR pairs is shown in Fig. 3. The DInSAR technique (Zebker et al. 1994) was then used to process all 18 available InSAR pairs (11 and seven for the LT and RT InSAR datasets, respectively), to generate 18 LOS deformation maps.

In the DInSAR processing, a multi-look operation of 1:2 pixels in the range and azimuth directions and least-squares-based filtering (Li et al. 2008) were carried out to suppress the phase noise of the interferograms. In addition, the 1-arc-second Shuttle Radar Topography Mission (SRTM) digital elevation model (DEM) was used to remove the topographic phase of the interferograms. The minimum cost flow algorithm (Costantini 1998; Chen and Zebker 2000) was then utilized to unwrap the differential interferograms. Finally, a quadratic polynomial model (Xu et al. 2014) was used to mitigate the phase ramps related to the long wavelength part of the atmospheric artifact screening and possible orbit errors.

3.3 Time-series 3-D displacement estimation

3.3.1 Track-based 3-D mining displacement generation

Although the available SAR images from two tracks were collected in this study, their imaging geometries were very similar (i.e., ascending orbits with a flight angle of about 350° and right looking with a nominal incidence angle of about 38°). In this case, time-series 3-D or even 2-D mining displacements cannot be accurately estimated using the MSBAS method (i.e., based on multi-track InSAR datasets only). A more detailed discussion on this issue is provided in Sect. 4.3. In addition, although the previous SGI method can also be applied to retrieve time-series 3-D displacements (but only for single-track InSAR datasets), it would result in a too coarse temporal resolution.

In this study, the prior deformation model [see Eq. (1)] was first applied to fully retrieve the adjacent-track 3-D mining displacements over the Yungang coal mining area from the 18 LOS deformation maps (generated as described in Sect. 3.2.2). The parameters of the prior model were as follows: (1) The flight angle and incidence angle of the LT and RT SAR images were about 349.7°/350° and 36.9°/39.7°, respectively; (2) the spatial resolution of the LOS deformation maps (after geocoding) was about 6 m in both the east and north directions; and (3) the mining depth of 250 m, the tangent of the major influence angle of 1.8, and the horizontal motion constant of 0.3 were designated, respectively (Hou and Zhang 2004).

3.3.2 Time-series 3-D displacement estimation

The reference dates of the generated multi-temporal 3-D displacement estimates were with reference to the dates of their own master images, rather than a unified one. Therefore, a GWLS solver was applied to adjust these adjacent 3-D mining displacement estimates, so that we could retrieve time-series 3-D mining displacements with respect to the same reference date (i.e., the earliest one in this study). To this end, we first chronologically ordered all the adjacent-track SAR images and assumed piece wise linear, that is, the 3-D displacement velocities between each two time-adjacent SAR images were constants. Secondly, the observation systems for the generated adjacent-track 3-D mining displacement measurements (described in Sect. 3.3.1) and the 3-D displacement velocity vectors were established, respectively. Thirdly, the developed mathematically rigorous weighting scheme and the GWLS solver were applied to solve the 3-D displacement velocity vectors. Finally, time-series 3-D displacements for the dates of all the adjacent-track SAR images, with respect to the earliest date of June 14, 2007, were estimated. The results are shown in Figs. 4, 5, and 6.

As can be seen from Figs. 4, 5, and 6, the 3-D displacement components of the mining area were small (with a maximum of 1.5 cm in the vertical direction, 2.1 cm in the east direction, and 3.4 cm in the north direction) before July 1, 2007. This can be attributed to the following reasons. Firstly, the size of the goaf (i.e., mined-out area) between June 14, 2007, and July 1, 2007 (see Fig. 2b) was small. Theoretically, under the same geomining conditions, the smaller the goaf, the smaller the mining-induced deformation magnitude (Peng et al. 1992). In addition, the small deformation magnitude would be further reduced by the supporting role of the overlying rock strata (Kratzsch 1983). As the working face continued to advance (as shown in Fig. 2b), the displacement basin gradually expanded and the maximum displacements

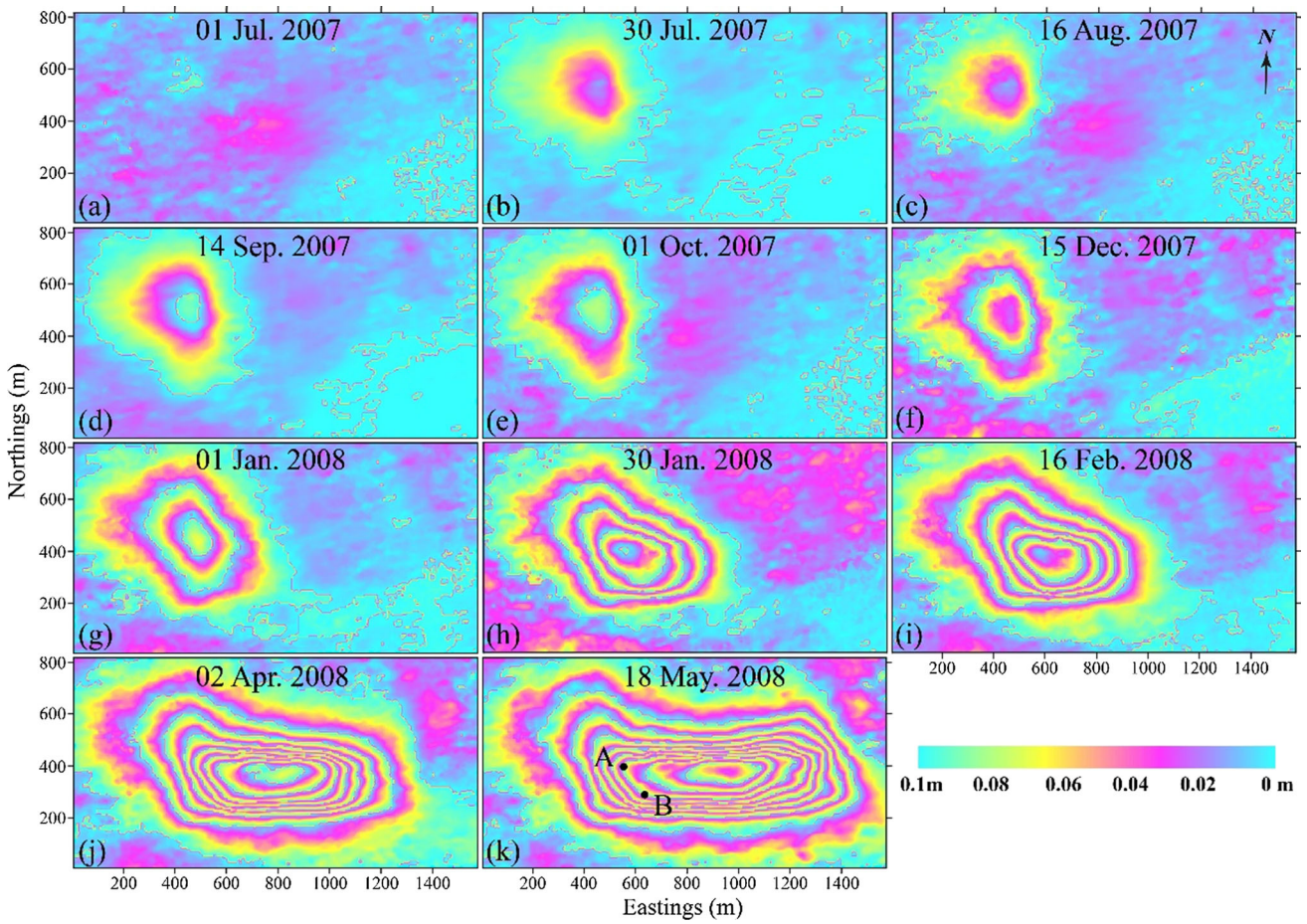

Fig. 4 MTI method estimated time-series vertical subsidence at the dates of the fused SAR images with respect to June 14, 2007. The estimated vertical subsidence is rewrapped by 0.1 m, i.e., one color cycle corresponds to 0.1 m vertical subsidence, for the sake of visualization

increased up to about 0.86 m, 0.37 m, and 0.16 m in the vertical, north, and east directions, respectively, over the following 10 months (see Figs. 4k, 5k, 6k).

Figure 7 shows the comparison between the time-series 3-D displacements derived by the proposed MTI method and the previous SGI method at the same SAR acquisition dates. As can be seen, the results solved by these two methods are in a good agreement, with an averaged mean of about 4×10^{-4} cm and STD of around 0.6 cm of their differences. Noting that, unlike the averaged mean, the averaged STD is not close to zero, possibly due to the fusion of adjacent-track InSAR measurements and the mathematically rigorous weighting scheme in the proposed MTI method. Unfortunately, due to the lack of in situ measurements of the 3-D displacements in the study area, an accuracy validation of the time-series 3-D mining displacement estimates with a densified temporal resolution could not be conducted in this study.

Even so, compared with the previous SGI-derived results presented in Yang et al. (2018a), the temporal resolution of the time-series 3-D displacement estimates in this study is dramatically reduced from the 54 days of Yang et al. (2018a) to 31 days, representing an improvement of about 42.6%. In doing so, more details of the spatio-temporal evolution patterns of the mining deformation in this coal mining area can be revealed from the results with a densified temporal resolution. This is of great importance for understanding and modeling the distinctive kinematics of the mining deformation and assessing mining-related geohazards in the Yungang coal mining area (see the detailed analysis in Sect. 4.1).

4 Discussion

4.1 Influence of the temporal resolution of time-series 3-D displacement estimates on dynamic displacement modeling and geohazard assessment

Mining-induced 3-D displacements are generally characterized by high nonlinearity in time (Peng et al. 1992), and the resulting geohazards (e.g., landslides) are also usually progressive (Kratzsch 1983). Therefore, the temporal

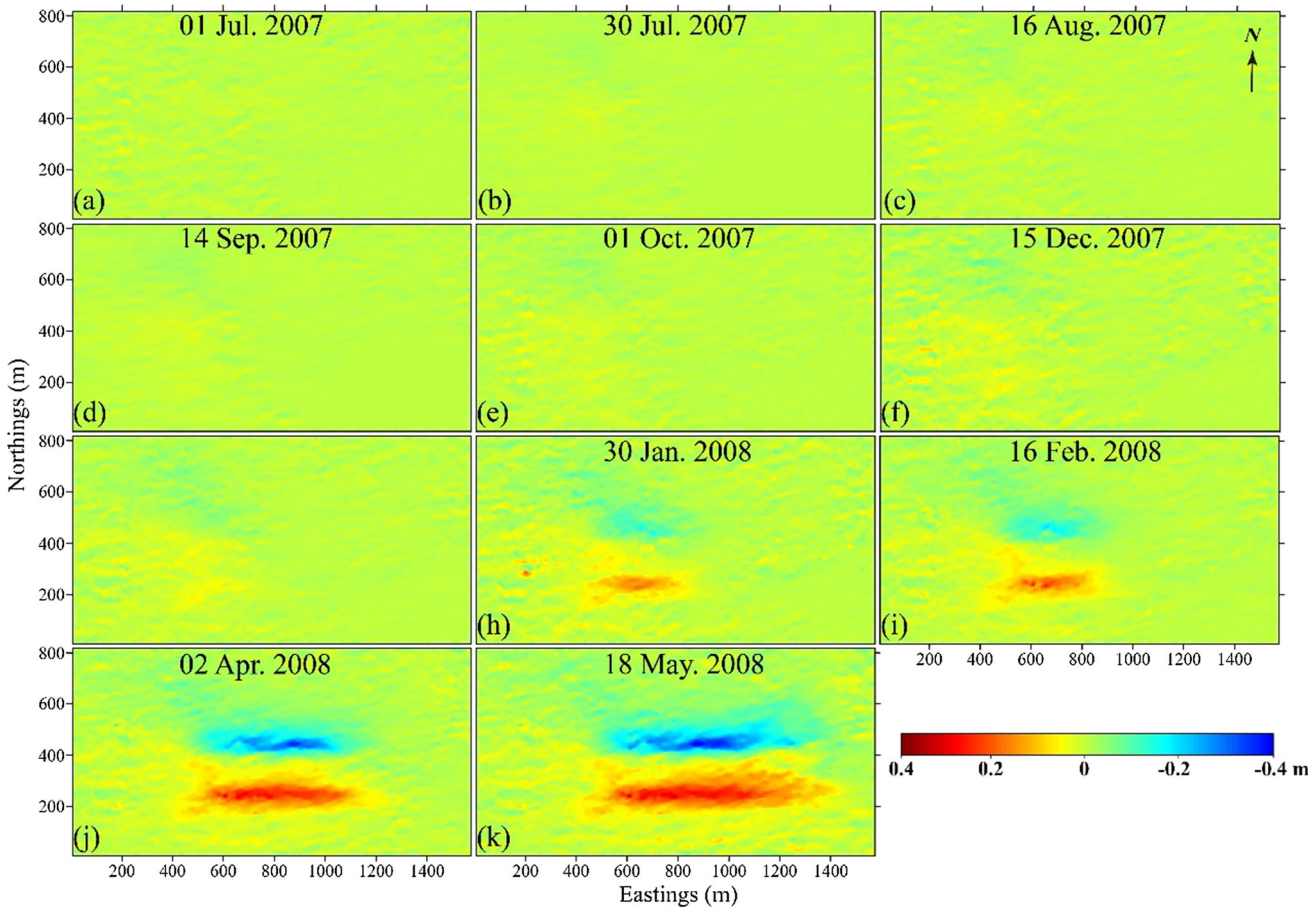

Fig. 5 MTI method derived time-series horizontal motion in the north direction at the dates of the fused SAR images with respect to June 14, 2007. Positive and negative values indicate the points moving toward the north and south directions, respectively

resolution of time-series 3-D displacements can have a significant influence on dynamic 3-D displacement modeling and mining-related geohazard assessment and control. These two issues are analyzed in detail with both simulated and real-data analyses in this section.

4.1.1 Simulation analysis

For simplicity, we take the mining-induced vertical subsidence at a single ground surface point as an example to analyze the influence of the temporal resolution of 3-D displacement estimates for mining deformation modeling and geohazard assessment. More specifically, we first simulated the time-series vertical subsidence using a logistic model that can suitably describe mining kinematic subsidence at a single surface point (Zhang et al. 2009; Yang et al. 2017b). The simulated dynamic subsidence, velocity, and acceleration obtained using the logistic model at this point are marked by the green lines in Fig. 8a–c. Secondly, time-series vertical subsidence estimates derived from the two InSAR datasets (called LT and RT in the following) were extracted from the logistic-simulated dynamic subsidence (hereinafter referred to as the *logistic-simulated time-series subsidence*). The temporal resolution of the extracted LT and RT time-series subsidence estimates was 46 days (i.e., the repeat cycle of the ALOS-1 satellite). In addition, Gaussian noise with a mean value of zero and a standard deviation (STD) of 3 cm was added to each of the LT and RT time-series subsidence estimates, to simulate time-series uncertainties (hereinafter called *LT* and *RT time-series subsidence observations*). The results are marked by the magenta stars and red asterisks in Fig. 8a and d, respectively.

To analyze the influence of the temporal resolution of the time-series subsidence observations on the deformation modeling, we first fitted the logistic model using the hybrid genetic algorithm and simplex algorithm (Yang et al. 2017b), based on the LT, RT, and LT + RT time-series subsidence observations, respectively. The results are plotted by the blue lines in Fig. 8a, d, g. For the sake of comparison, the fitted velocity and acceleration at this point are shown as blue lines in Fig. 8b, e, h, as well as 8c, f, i, respectively. The root-mean-square errors (RMSEs) between the logistic-simulated and

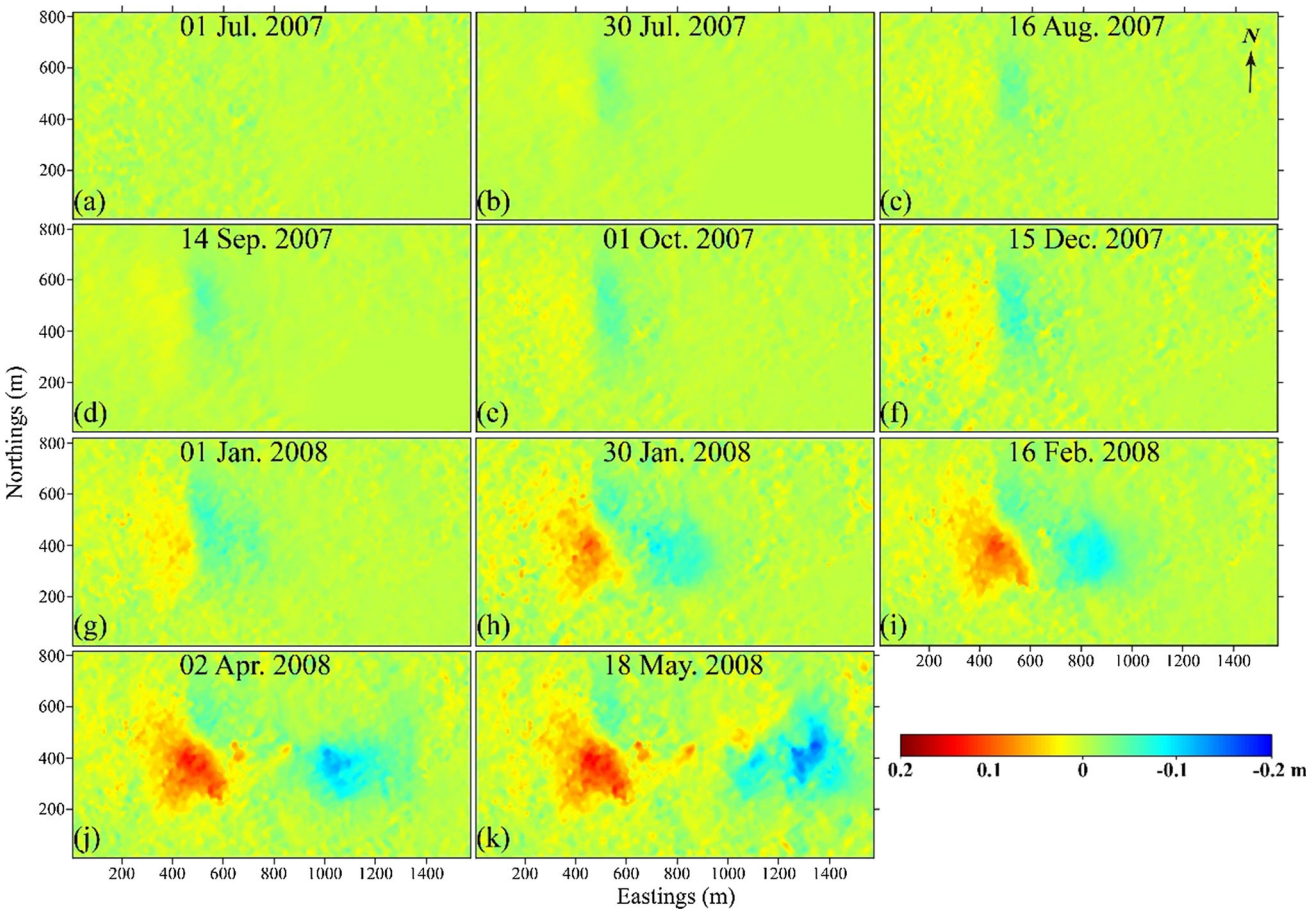

Fig. 6 MTI method derived time-series horizontal motion in the east direction at the dates of the fused SAR images with respect to June 14, 2007. Positive and negative values indicate the points moving toward the east and west directions, respectively

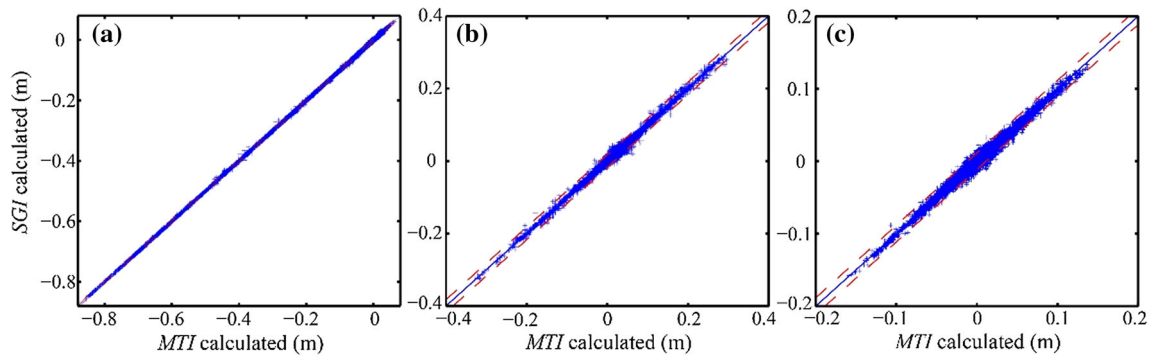

Fig. 7 Comparison between the time-series 3-D (vertical, north, and east directions) displacements derived by the MTI method and the SGI method at the same SAR acquisition dates

the fitted time-series subsidence, velocity, and acceleration are listed in Table 1.

As can be seen in Fig. 8, the fitted dynamic subsidence curves based on the LT and RT time-series subsidence observations show obvious discrepancy with the logistic-simulated one, with a mean relative error of about 3.5% to the maximum vertical subsidence. This discrepancy becomes more significant when it comes to the dynamic subsidence velocity and acceleration to the maximum velocity and acceleration (i.e., with mean relative errors of about 7.5% and 17.4%, respectively). If the real mining deformation kinematics could not be revealed, the subsequent assessment and effective control of mining-related geohazards would be impeded. For instance, mining-induced structural damage controlling

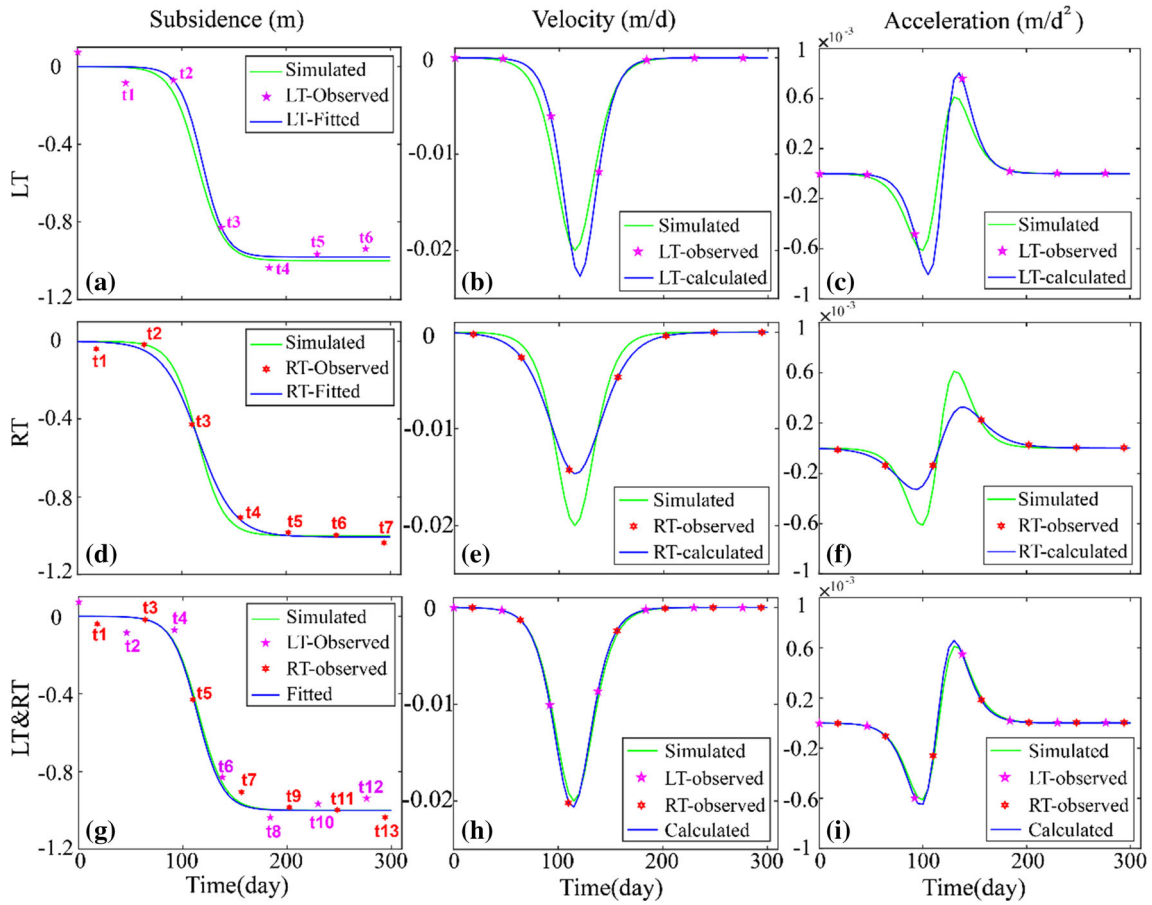

Fig. 8 Comparison between the simulated and the fitted subsidence, velocity, and acceleration from the time-series observations of **a**–**c** LT only, **d**–**f** RT only, and **g**–**i** LT and RT together

Table 1 RMSEs between the simulated and the fitted time-series subsidence, velocity, and acceleration

Dataset	Subsidence ($\times 10^{-2}$m)	Velocity ($\times 10^{-3}$ m/day)	Acceleration ($\times 10^{-5}$ m/day^2)
LT	3.8	1.4	10.5
RT	3.1	1.6	10.8
Fused LT&RT	0.9	0.3	2.6

measures should be taken before the date of the maximum subsidence velocity. However, if this estimated date was not within the optimized date range (especially when the estimated date is delayed) due to the coarse temporal resolution observations (e.g., see Fig. 8b), the performance of the damage control measures would be dramatically degraded, or it may even cause these measures not to work.

In fact, the main reason for such large errors existing in the LT- and RT-fitted dynamic subsidence is due to the fact that mining-induced time-series subsidence at a single ground surface point commonly follows an "S" shape (or sigmoid curve) (Yang et al. 2017b), and subsidence observations with a poor temporal resolution cannot constrain the "S" shape (Mo et al. 2010), causing large errors in the mining displacement modeling. However, if the time-series subsidence observations derived from the LT and RT SAR images (see Fig. 8g) are applied to fit the logistic model, the relative errors of the fitted subsidence, velocity, and acceleration are decreased from 3.5 to 0.9%, from 7.5 to 1.8%, and from 17.4 to 4.2%, respectively. These results suggest that time-series 3-D displacement observations with a high temporal resolution are critical for kinematics modeling and mining-related geohazard control.

4.1.2 Real-data analysis

Two ground surface points of the Yungang coal mining area, namely A and B (marked by the black circles in Fig. 4k), were selected to analyze the influence of the temporal resolution on 3-D deformation kinematics modeling and mining-related geohazard assessment and control. To this end, we first unify the reference benchmark of the SGI-derived (marked by the blue asterisks in Fig. 9) and MTI-derived time-series sub-

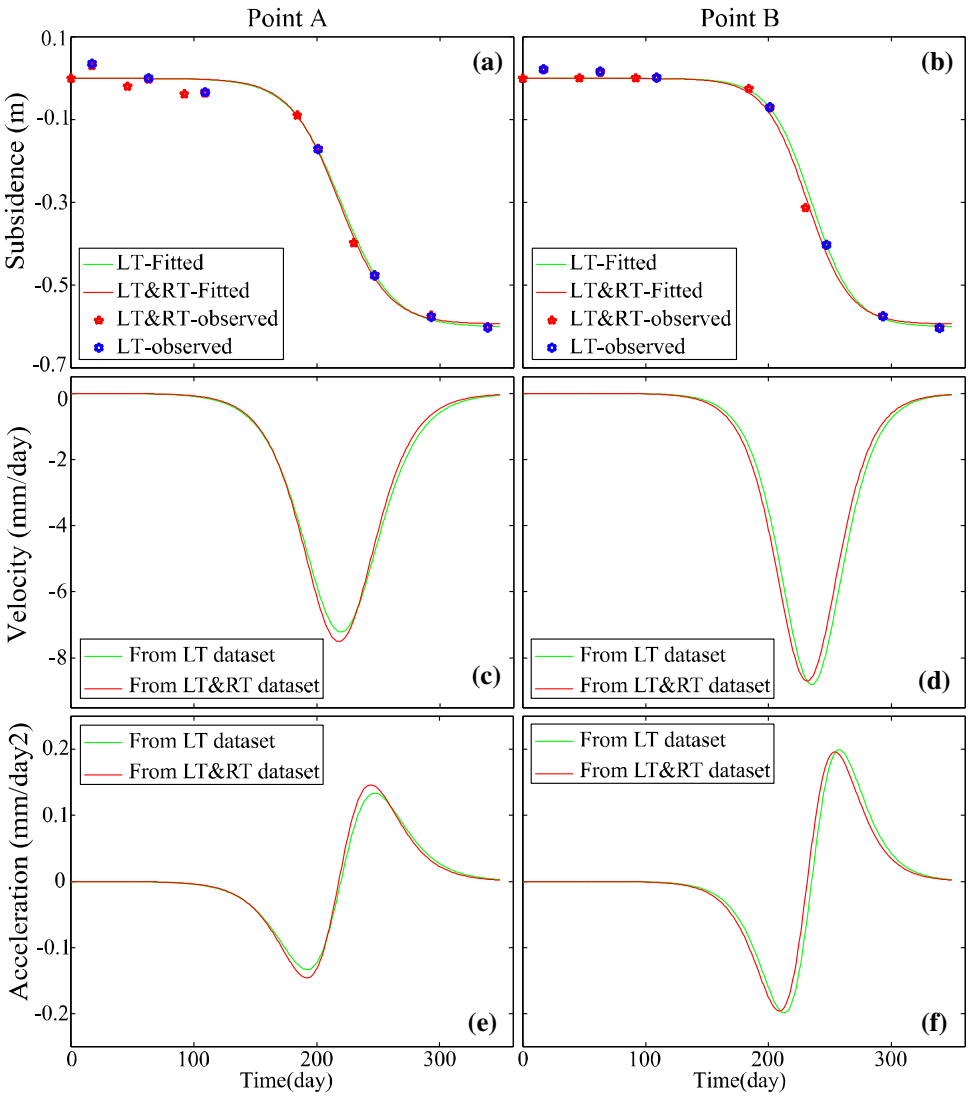

Fig. 9 Fitted subsidence models of points A and B, and their subsidence, velocity, and acceleration curves

sidence observations (marked by the red stars in Fig. 9) by using the average of the difference values between the data of the same acquisition time. After that, the dynamic subsidence at points A and B is fitted using the logistic model based on the reference benchmark unified SGI-derived and MTI-derived time-series subsidence observations, respectively. The fitted dynamic subsidence, velocity, and acceleration are marked by the green and red lines in Fig. 9. It can be seen from Fig. 9 that the modeled maximum subsidence velocity and acceleration based on the SGI-derived results at point A are smaller than those based on the MTI-derived ones. In addition, the fitted dates where the maximum subsidence velocity and acceleration occur at both points A and B based on the SGI-derived time-series subsidence are all about eight days later than those based on the MTI-derived values. These results indicate that higher temporal resolution time-series subsidence observations can offer more details on mining subsidence evolution in the temporal domain, facilitating kinematics modeling. In addition, higher temporal resolution time-series subsidence observations can help us to accurately determine some essential information for geohazard control (e.g., the date where the maximum subsidence velocity occurs).

Figure 10 plots a comparison of the time-series horizontal motions in the east direction at point A, as derived by the SGI and MTI methods. For a fair comparison, we also unify the reference benchmark of the SGI-derived and the MTI-derived results by using the average of the difference values between the data of the same acquisition time. As can be seen, due to the poor temporal resolution of the SGI-derived observations (blue asterisks), the maximum horizontal motion (marked by the magenta ellipse) at this point is missed, but is captured by the MTI-derived observations. Since mining-induced structural damage is very sensitive to horizontal motions, the missing of the maximum horizontal motion in the east direction would result in underestimation of the structural damage

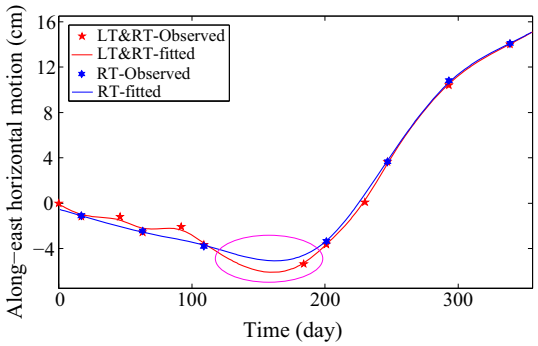

Fig. 10 Time-series horizontal displacements in the east direction at point A

(Yang et al. 2018b), imposing an extra threat to human lives and properties. Consequently, for geohazard assessment, it is essential to obtain time-series 3-D displacements with a higher temporal resolution.

4.2 Influence of the weighting scheme on time-series 3-D displacement estimation

In this paper, a new weighting scheme is proposed based on the stochastic model of interferometric phase variance. Compared with the empirical weighting function of the cubic of coherence (hereafter referred to as CCM) used in the SGI method, the newly developed weighting scheme is theoretically more rigorous. In this section, the influence of these two weighting schemes on the accuracy of time-series 3-D displacement estimates is analyzed.

Figure 11a shows a comparison between the CCM-estimated weighting curve and the reciprocal of the normalized theoretical variance curves of the InSAR phase [i.e., estimated by Eq. (4)]. As can be seen, the CCM-based curve is an empirical weighting function, which cannot perfectly match any of the normalized variance curves in Fig. 11a. In fact, it can be observed from Fig. 11a that the CCM-based curve is a trade-off for weighting the normalized theoretical variance curves at multi-look numbers from eight to 14. This means that the CCM weighting scheme is unable to precisely suppress the error propagation of InSAR deformation observations, especially for InSAR processing with small multi-look numbers (e.g., two in Fig. 11a).

In contrast, the new weighting scheme proposed in this paper is based on Eq. (4) and takes both coherence and multi-look number into account. This implies that the theoretical errors of InSAR-derived LOS deformation observations at different multi-look numbers are rigorously considered. The law of error propagation is then introduced to deduce the theoretical variance–covariance matrices of the 3-D mining displacement estimates, forward guiding the construction of the weighting matrix to obtain the GWLS solution for the time-series 3-D mining displacements (see Sect. 2.2.2). Theoretically, the weighting scheme proposed in this paper is more rigorous than the CCM one and can thus more effectively suppress the error propagation of InSAR observations.

A simulation experiment was carried out to quantitatively analyze the accuracy improvement of time-series 3-D displacements estimated by the proposed weighting scheme, compared with those estimated by the previous CCM weighting scheme. More specifically, we first extracted coherence datasets with the pixel dimensions of 40×40 from all the available LT and RT InSAR pairs (see Sect. 3). The variance–covariance matrices of the 3-D mining displacements were then obtained using the method described in Sect. 2.2.2, by setting the multi-look numbers from two to 14. Finally, the uncertainties of the time-series 3-D displacements estimated by the proposed method at different multi-look numbers were theoretically determined according to the law of error propagation. For the sake of comparison, the theoretical uncertainties of the time-series 3-D displacements estimated by the CCM weighting scheme were also determined.

Figure 11b plots the accuracy improvement of the time-series subsidence estimated by the proposed weighting scheme compared with that estimated by the CCM scheme. As is shown, the accuracy of the time-series subsidence can be improved using the proposed weighting scheme, but the improvement gradually decreases from about 23 to 13% with the increase in the multi-look number from two to 14. This is mainly because the CCM scheme is only a trade-off for

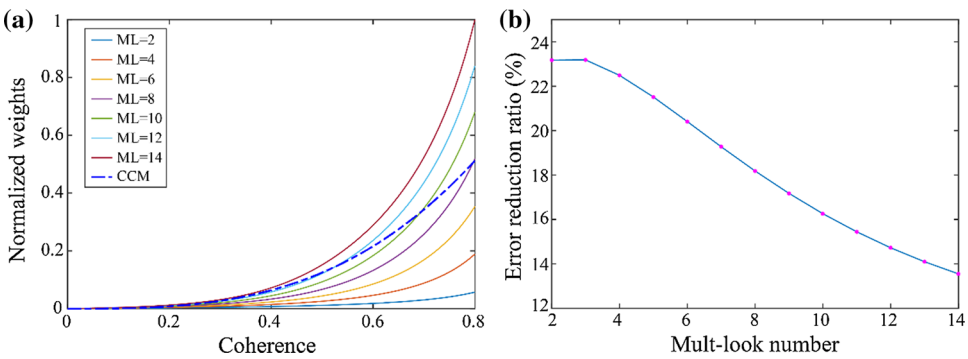

Fig. 11 **a** Comparison between the CCM-based weighting curve (blue dashed line) and the reciprocal of the theoretical interferometric phase variances at different multi-look (ML) numbers. **(b)** Accuracy improvement of the time-series 3-D displacements estimated by the proposed weighting scheme compared with those estimated by the CCM weighting scheme

weighting phase variances at multi-look numbers from eight to 14, and it shows a poor performance in variance suppression for small multi-look numbers. These results suggest that the weighting scheme can significantly affect the accuracy of time-series 3-D displacement estimates, and the theoretically rigorous weighting scheme proposed in this paper can effectively improve the accuracy of the estimates, especially in the case of small multi-look numbers.

4.3 Superiority of the proposed method over the traditional MSBAS method for adjacent-track InSAR datasets

In this study, ALOS PALSAR-1 datasets from two spatially adjacent tracks were applied to retrieve time-series 3-D displacements with a high temporal resolution, with the assistance of a prior deformation model. Theoretically, two SAR datasets from different imaging geometries are potentially able to retrieve time-series 2-D displacements or deformation velocities in the vertical and east (or quasi-east) directions by neglecting the contribution of the horizontal motion in the north direction to LOS deformation using the core idea of the MSBAS method (Samsonov et al. 2013). To date, some successful cases for volcanic eruption events and post-mining activity have been reported based on ascending and descending SAR datasets (Manzo et al. 2006; Samsonov and d'Oreye 2012; Samsonov et al. 2013) and adjacent-track SAR datasets with significantly different imaging geometries (Gourmelen et al. 2007).

The superiority of the proposed method over the traditional MSBAS method for 2-D mining displacement estimation in vertical and east directions was analyzed based on the selected adjacent-track ALOS PALSAR-1 datasets in the real-data experiment (see Sect. 3.2). More specifically, we first simulated time-series 3-D mining displacements with the probability integral method (a widely used mining deformation model) (Guo and Chai 2013; Yang et al. 2018b) and then projected them to each LOS direction of the used LT and RT PALSAR-1 images. The simulated time-series 2-D displacements in the vertical and east directions are shown in Fig. 12Ai and Di ($i = [1, 2, \ldots, 8]$), respectively. Gaussian noise with a mean value of zero and an STD of 1.5 cm was then generated and added to each of the projected LOS displacement maps. Small-baseline InSAR pairs and LOS deformation observations were also generated based on the projected LOS displacements with Gaussian noise. Finally, the time-series 2-D displacements in the vertical and east directions were estimated from the adjacent-track SAR datasets by ignoring the motion in the north direction (i.e., using the MSBAS method; for more details, see Samsonov et al. 2013). The results are shown in Fig. 12Ci and Fi, respectively. In addition, the corresponding time-series 2-D displacements estimated by the MTI-based method are plotted in Fig. 12Bi and Ei, for the sake of a comparison.

It can be seen from Fig. 12 that the time-series 2-D displacement estimates with the motion in the north direction ignored are dominated by noise, with RMSEs of 28.9 and 37.1 cm in the vertical and east directions, respectively. Such errors are about 19 and 25 times the STD of the generated Gaussian noise to the LOS observations. This implies that time-series 2-D mining displacements cannot be accurately estimated based on the selected adjacent-track ALOS PALSAR-1 datasets used in this study if the existing MSBAS method is used. The main reason for this is that the imaging geometries of the used LT and RT ALOS PALSAR-1 datasets are very similar, causing near equivalence between the unit projection vectors of the displacements in the vertical and east directions (see Hanssen 2001 for more details) for the LT and RT SAR images (i.e., $[0.7993, -0.5913]$ and $[0.7693, -0.6294]$, respectively). This means that the equation system for solving time-series 2-D displacements is ill-posed, thus resulting in large errors in the time-series 2-D displacement estimates. However, as can be seen in Fig. 12, the results estimated by the MTI method show a good agreement with the simulated ones, with RMSEs of about 0.25 cm and 3 cm in the vertical and east directions, respectively. Compared with the MSBAS-estimated results, the accuracy of the MTI method estimated results is improved by 99% and 92%, respectively.

In addition, we validated the superiority of the MTI method over the previous MSBAS method for mining-induced time-series 2-D displacement estimation with real datasets described in Sect. 3.2. Note that only the time period that both LT and RT SAR images expand (i.e., from July 1, 2007 to January 30, 2008) was selected for the use of the MSBAS method. The results are shown in Fig. 13. As can be seen, similar to the previous simulation results, the MSBAS-derived time-series 2-D mining displacements are much noisy than the MTI-derived ones. Although no in situ measurements are applied to quantitatively evaluate the accuracy differences of these two result sets, the MTI-derived estimates are theoretically more reliable than the MSBAS-derived ones according to mining subsidence theory (Kratzsch 1983). Both the simulated and real experiments indicate that the proposed method has a good superiority over the traditional MSBAS method for retrieving 2-D mining displacements from spatially adjacent-track SAR images.

It is noted that only Gaussian noise is considered in this section, and which may be not realistic for InSAR measurements that possibly include non-random errors (e.g., atmospheric phase and orbital error residuals after correction). Nevertheless, the error propagation way is theoretically the same for a certain system, whatever the error types are (e.g., random or non-random). Consequently, the superiority test of the proposed MTI method over the traditional MSBAS

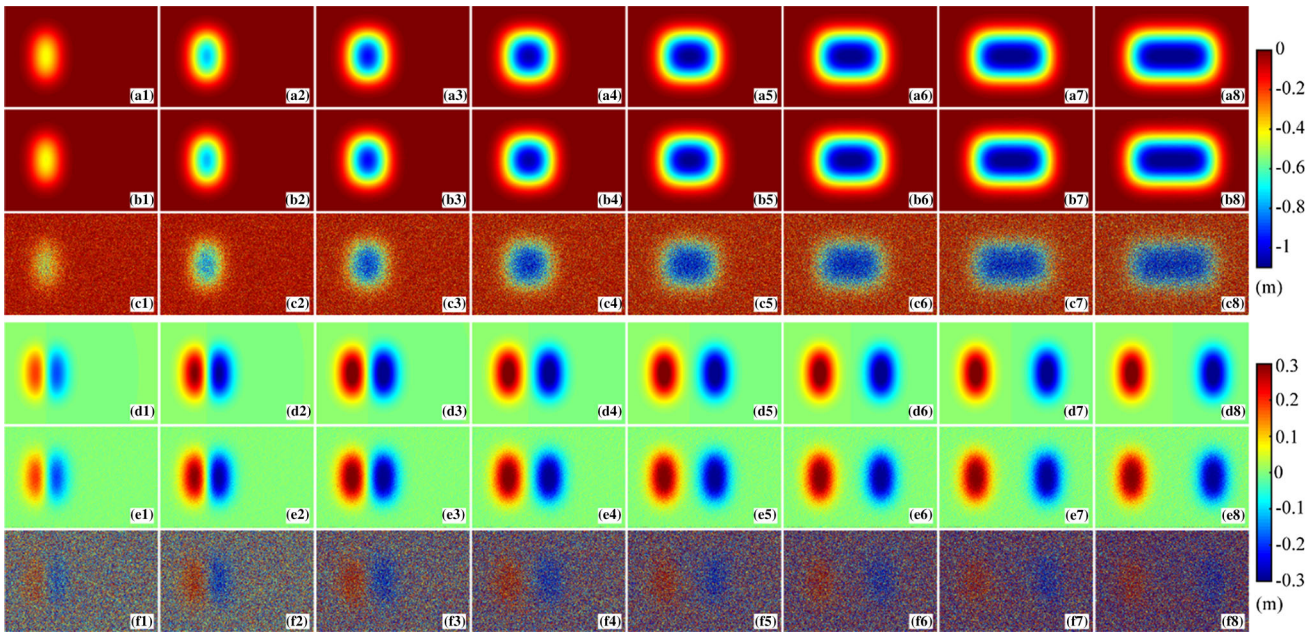

Fig. 12 Time-series 2-D displacements in the vertical and east directions simulated by the probability integral method (i.e., **A1**–**A8** and **D1**–**D8**), the results estimated by the MTI method (i.e., **B1**–**B8** and **E1**–**E8**), and the results estimated by the MSBAS method (i.e., **C1**–**C8** and **F1**–**F8**), respectively

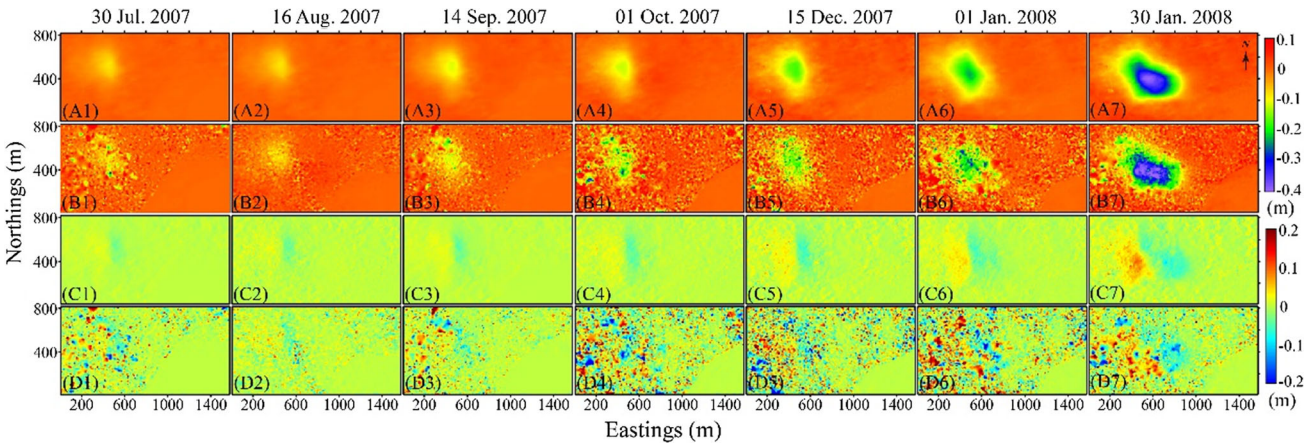

Fig. 13 Time-series 2-D mining displacements in the vertical and east directions estimated by the MTI method (i.e., **A1**–**A7** and **C1**–**C7**), and the results estimated by the MSBAS method (i.e., **B1**–**B7** and **D1**–**D7**), respectively

method for 2-D mining displacement estimation is reasonable, even though only Gaussian noise is considered in this section (Fig. 12).

5 Conclusions

In this paper, we have presented an approach to estimate time-series 3-D mining displacements by fusing multi-track InSAR datasets, with the assistance of a prior deformation model. The main aim of the proposed approach is to enhance the temporal resolution of the previous SGI-derived time-series 3-D mining displacements from single-track InSAR datasets. Twelve ascending ALOS PALSAR-1 images from two spatially adjacent tracks over the Yungang mining area of China were selected to test the proposed MTI-based method. The results showed that, compared to the previous SGI-derived results, the temporal resolution of the time-series 3-D mining displacements estimated by the MTI-based method is improved by around 45.5%. Time-series 3-D mining displacement measurements with a high spatio-temporal resolution are essential for mining deformation kinematics modeling and mining-induced geohazard assessment and control.

In addition, a new weighting scheme has been proposed for improving the GWLS solutions of time-series 3-D displacements. Compared with the empirical CCM-based weighting scheme used in the previous SGI method, the newly developed scheme is mathematically rigorous, so that it can effectively suppress the error propagation of InSAR deformation observations and improve the accuracy of time-series 3-D displacement estimates. Finally, the superiority of the proposed method over the traditional MSBAS method (a typical multi-track-based method) for retrieving time-series 2-D mining displacements was investigated based on the two selected adjacent-track SAR datasets considered in this study. The results indicated that the accuracies of the time-series 2-D displacement estimates in the vertical and east directions are both very poor for the MSBAS method, due to the similarity of the imaging geometries of the selected adjacent-track SAR datasets. However, the accuracy can be dramatically improved by 99% and 92% in the vertical and east directions, respectively, if the MTI-based method is applied to retrieve the time-series 3-D displacements.

However, we should stress that only a real-data case study was carried out to test the MTI-based method in this study using an adjacent-track InSAR dataset, and accuracy validation of the retrieved time-series 3-D displacement estimates could not be conducted, due to the lack of in situ GPS or leveling deformation measurements. Therefore, in our future study, we will further test the MTI-based method in more study areas and more multi-track InSAR datasets, we will validate the accuracy of the results, and we will explore the potential of the core idea of the MTI-based method in other applications of geophysical deformation event monitoring.

Acknowledgements This work was partly supported by the National Key R&D Program of China (No. 2018YFC1503603), the Leading Talents Plan of Central South University (Grant Number 506030101), the National Natural Science Foundation of China (Nos. 41904005, 41474008 and 41474007), and the Fundamental Research Funds for the Central Universities of Central South University (2018zzts685). The authors would also like to thank the Japan Aerospace Exploration Agency (JAXA) for providing the PALSAR images over study areas (No. P3214002).

Author's contributions ZY and ZL provided the initial idea and designed the experiments for this study; YW carried out the designed experiments; YW and ZY wrote the manuscript; JZ and LW analyzed the data and helped with the writing. All authors reviewed the manuscript.

Data availability The ALOS PALSAR SAR images are available in the JAXA repository, https://auig2.jaxa.jp/ips/home. The SRTM DEM is obtained from the USGS EarthExplorer, https://earthexplorer.usgs.gov.

References

Berardino P, Fornaro G, Lanari R, Sansosti E (2002) A new algorithm for surface deformation monitoring based on small baseline differential SAR interferograms. IEEE Trans Geosci Remote Sens 40(11):2375–2383. https://doi.org/10.1109/TGRS.2002.803792

Campbell SL, Meyer CD (1979) Generalized inverses of linear transformations. Pitman Publishing Limited, London

Catalao J, Nico G, Hanssen R, Catita C (2011) Merging GPS and atmospherically corrected InSAR data to map 3-D terrain displacement velocity. IEEE Trans Geosci Remote Sens 49(6):2354–2360. https://doi.org/10.1109/TGRS.2010.2091963

Chaussard E, Wdowinski S, Cabral-Cano E, Amelung F (2014) Land subsidence in central Mexico detected by ALOS InSAR time-series. Remote Sens Environ 140:94–106. https://doi.org/10.1016/j.rse.2013.08.038

Chen CW, Zebker HA (2000) Network approaches to two-dimensional phase unwrapping: intractability and two new algorithms. J Opt Soc Am A Opt Image Sci Vis 17(3):401–414. https://doi.org/10.1364/JOSAA.17.000401

Costantini M (1998) A novel phase unwrapping method based on network programming. IEEE Trans Geosci Remote Sens 36(3):813–821. https://doi.org/10.1109/36.673674

Dou LM, Mu ZL, Li ZL, Cao AY, Gong SY (2014) Research progress of monitoring, forecasting, and prevention of rockburst in underground coal mining in China. Int J Coal Sci Technol 1(3):278–288. https://doi.org/10.1007/s40789-014-0044-z

Fournier TJ, Pritchard ME, Riddick SN (2010) Duration, magnitude, and frequency of subaerial volcano deformation events: new results from Latin America using InSAR and a global synthesis. Geochem Geophys Geosyst 11(1):1–29. https://doi.org/10.1029/2009GC002558

Gourmelen N, Amelung F, Casu F, Manzo M, Lanari R (2007) Mining-related ground deformation in Crescent Valley, Nevada: Implications for sparse GPS networks. Geophys Res Lett. https://doi.org/10.1029/2007gl029427

Guo ZZ, Chai HB (2013) Coal mining subsidence. China Coal Industry Publishing House, Beijing

Hanssen RF (2001) Radar interferometry: data interpretation and error analysis. Springer, Berlin

Hou ZY, Zhang YH (2004) Movement law of coal mining subsidence surface ground in Datong Mining Area. Coal Sci Technol 2(32):50–53. https://doi.org/10.13199/j.cst.2004.02.52.houzhy.017

Hu J, Li ZW, Sun Q, Zhu JJ, Ding XL (2012) Three-dimensional surface displacements from InSAR and GPS measurements with variance component estimation. IEEE Geosci Remote Sens Lett 9(4):754–758. https://doi.org/10.1109/LGRS.2011.2181154

Jia X, Ma C, Zhao A (2010) Environmental investigation and evaluation of land subsidence in the Datong coalfield based on InSAR technology. Acta Geol Sin 82(5):1035–1044. https://doi.org/10.1111/j.1755-6724.2008.tb00660.x

Kratzsch H (1983) Mining subsidence engineering. Springer, New York

Li ZW, Ding XL, Zheng DW, Huang C (2008) Least squares-based filter for remote sensing image noise reduction. IEEE Trans Geosci Remote Sens 46(7):2044–2049. https://doi.org/10.1109/TGRS.2008.916981

Li ZW, Yang ZF, Zhu JJ, Hu J, Wang YJ, Li PX, Chen GL (2015) Retrieving three-dimensional displacement fields of mining areas from a single InSAR pair. J Geod 89(1):17–32. https://doi.org/10.1007/s00190-014-0757-1

Liu XG, Xu WB (2019) Logarithmic model joint inversion method for coseismic and postseismic slip: Application to the 2017 Mw 7.3 Sarpol Zahāb earthquake, Iran. J Geophy Res Solid Earth 124:12034–12052. https://doi.org/10.1029/2019JB017953

Liu JH, Hu J, Li ZW, Zhu JJ, Sun Q, Gan J (2018) A method for measuring 3-D surface deformations with InSAR based on strain model and variance component estimation. IEEE Trans Geosci Remote Sens 56(1):239–250. https://doi.org/10.1109/TGRS.2017.2745576

Lu Z, Dzurisin D, Biggs J, Wicks C Jr, McNutt S (2010) Ground surface deformation patterns, magma supply, and magma storage at Okmok volcano, Alaska, from InSAR analysis: 1. Intereruption deformation, 1997–2008. J Geophys Res 115:B00B02. https://doi.org/10.1029/2009JB006969

Lu CP, Dou LM, Zhang N, Xue JH, Wang XN, Liu H, Zhang JW (2013) Microseismic frequency-spectrum evolutionary rule of rockburst triggered by roof fall. Int J Rock Mech Min 64:6–16. https://doi.org/10.1016/j.ijrmms.2013.08.022

Manzo M, Ricciardi GP, Casu F, Ventura G, Zeni G, Borgstrom S, Berardino P, Gaudio C, Lanari R (2006) Surface deformation analysis in the Ischia Island (Italy) based on spaceborne radar interferometry. J Volcanol Geotherm Res 151(4):399–416. https://doi.org/10.1016/j.jvolgeores.2005.09.010

Marschalko M, Yilmaz I, Bednárik M, Kubečka K (2012) Influence of underground mining activities on the slope deformation genesis: Doubrava Vrchovec, Doubrava Ujala and Staric case studies from Czech Republic. Eng Geol 147:37–51. https://doi.org/10.1016/j.enggeo.2012.07.014

Mo Y, Yue H, Hu B, Wu BP (2010) A study of logistic equation applied to predicting ground settlement induced by subway tunneling work. Chin J Eng Geophys 7(1):115–119. https://doi.org/10.3969/j.issn.1672-7940.2010.01.024

Mohr JJ, Reeh N, Madsen Søren N (1998) Three-dimensional glacial flow and surface elevation measured with radar interferometry. Nature 391(6664):273–276. https://doi.org/10.1038/34635

Neri M, Casu F, Acocella V, Solaro G, Pepe S, Berardino P, Sansosti E, Caltabiano T, Lundgren P, Lanari R (2009) Deformation and eruptions at Mt. Etna (Italy): a lesson from 15 years of observations. Geophys Res Lett 36(2): L02309. https://doi.org/10.1029/2008GL036151

Peng SS, Ma WM, Zhong WL (1992) Surface subsidence engineering. Society for Mining, Metallurgy, and Exploration, Colorado

Reddish DJ, Whittaker BN (2012) Subsidence: occurrence, prediction and control. Elsevier, Amsterdam

Ryder I, Parsons B, Wright TJ, Funning GJ (2007) Post-seismic motion following the 1997 Manyi (Tibet) earthquake: InSAR observations and modelling. Geophys J Int 169(3):1009–1027. https://doi.org/10.1111/j.1365-246X.2006.03312.x

Samsonov S, d'Oreye N (2012) Multidimensional time-series analysis of ground deformation from multiple InSAR data sets applied to Virunga Volcanic Province. Geophys J Int 191:1095–1108. https://doi.org/10.1111/j.1365-246X.2012.05669.x

Samsonov S, d'Oreye N, Smets B (2013) Ground deformation associated with post-mining activity at the French–German border revealed by novel InSAR time series method. Int J Appl Earth Obs Geoinf 23:142–154. https://doi.org/10.1016/j.jag.2012.12.008

Xie H, Zhou HW (2008) Application of fractal theory to top-coal caving. Chaos Soliton Fractals 36:797–807. https://doi.org/10.1016/j.chaos.2006.07.024

Xu B, Li ZW, Wang QJ, Jiang M, Zhu JJ, Ding XL (2014) A refined strategy for removing composite errors of SAR interferogram. IEEE Geosci Remote Sens Lett 11(1):143–147. https://doi.org/10.1109/LGRS.2013.2250903

Yang ZF, Li ZW, Zhu JJ, Preusse A, Yi HW, Wang YJ, Papst M (2017a) An extension of the InSAR-based probability integral method and its application for predicting 3-D mining-induced displacements under different extraction conditions. IEEE Trans Geosci Remote Sens 99:1–11. https://doi.org/10.1109/TGRS.2017.2682192

Yang ZF, Li ZW, Zhu JJ, Yi HW, Hu J, Feng GC (2017b) Deriving dynamic subsidence of coal mining areas using InSAR and logistic model. Remote Sens 9(2):125. https://doi.org/10.3390/rs9020125

Yang ZF, Li ZW, Zhu JJ, Feng GC, Wang QJ, Hu J, Wang CC (2018a) Deriving time-series three-dimensional displacements of mining areas from a single-geometry InSAR dataset. J Geod 92(5):529–544. https://doi.org/10.1007/s00190-017-1079-x

Yang ZF, Li ZW, Zhu JJ, Preusse A, Hu J, Feng GC, Wang YJ, Papst M (2018b) An InSAR-based temporal probability integral method and its application for predicting mining-induced dynamic deformations and assessing progressive damage to surface buildings. IEEE J STARS 11(2):472–484. https://doi.org/10.1109/JSTARS.2018.2789341

Yang ZF, Li ZW, Zhu JJ, Wang YD, Wu LX (2020) Use of SAR/InSAR in mining deformation monitoring, parameter inversion, and forward prediction: a review. IEEE Geosci Remote Sens Min 8(1):71–90. https://doi.org/10.1109/MGRS.2019.2954824

Zebker HA, Rosen PA, Goldstein RM, Gabriel A, Werner CL (1994) On the derivation of coseismic displacement fields using differential radar interferometry: the Landers earthquake. J Geophys Res 99(B10):19617–19634. https://doi.org/10.1029/94JB01179

Zhang WZ, Zou YF, Ren XF (2009) Research on logistic model in forecasting subsidence single-point during mining. J Min Saf Eng 26(4):486–489. https://doi.org/10.3969/j.issn.1673-3363.2009.04.019

Zhao CY, Zhang Q, Yang CS, Zou WB (2011) Integration of MODIS data and short baseline subset (SBAS) technique for land subsidence monitoring in Datong, China. J Geodyn 52(1):16–23. https://doi.org/10.1016/j.jog.2010.11.004

Zhao Y, Jiang Y, Wang T, Gao F, Xie S (2012) Features of microseismic events and precursors of rock burst in underground coal mining with hard roof. J China Coal Soc 37(12):1960–1966. https://doi.org/10.13225/j.cnki.jccs.2012.12.010

Zhao R, Li ZW, Feng GC, Wang QJ, Hu J (2016) Monitoring surface deformation over permafrost with an improved SBAS-InSAR algorithm: with emphasis on climatic factors modeling. Remote Sens Environ 184:276–287. https://doi.org/10.1016/j.rse.2016.07.019

Zhu ZJ (2015) Hard roof movement feature and fully mechanized top-coal caving face's influence on strata behavior in Datong mining area. Ph.D. Thesis, Liaoning Technical University, Fuxin, Liaoning, China